Optimizing Performance of Antenna Arrays with Clustered Fractal Shapes for Multiband Applications

Jafar Ramadhan Mohammed and Dalia Ahmad Al-Khafaf

Ninevah University, Mosul, Iraq

https://doi.org/10.26636/jtit.2024.1.1456

Abstract — Fractal antennas are mainly used in multiband applications. However, these types of arrays suffer from numerous disadvantages, such as high sidelobe levels, low directivity, poor taper efficiency, and high design computational complexity. In this paper, the conventional fractal procedures are redesigned and efficient clustered subarrays are deployed, such that their multiband properties are maintained while simultaneously achieving significant improvements in radiation characteristics. A genetic optimization algorithm is used to find the optimal clustered fractal shapes and their associated amplitude distributions, such that the sidelobe levels are minimized at the narrower beam width, i.e. maximum feasible directivity. Since the optimization process is carried out at the clustered level, it can be represented by merely a few variables, which solves the problem of time intensity. Simulation results confirm the superiority of the proposed clustered fractal array, where the sidelobe level has been reduced to more than –10 dB over a wide range of frequencies. Directivity and taper efficiency have been improved by more than 6 dB and 50%, respectively, in comparison to the parameters of conventional, original fractal arrays. Moreover, the proposed fractal array pattern offers an additional advantage, as it is capable of wide sidelobe nulling at some undesired directions.

Keywords — array pattern optimization, clustered elements, fractal array antennas, multiband, Sierpinski carpet fractal array

1. Introduction

Larger antenna arrays play an important role in 5G/6G and beyond applications, as each receiver device may accommodate a larger number of antenna elements operating at mmWave frequencies. In addition to providing high directivity and good beamforming capabilities, these large arrays come with many limitations affecting their implementation. These include complex feeding networks, high cost, and narrow band operation. For multiband applications, fractal antenna arrays were found to be a good alternative [1]–[2]. In general, fractal antennas are self-similar geometries with the same structure repeating over different scales. Each scale corresponds to a specific frequency band.

In the literature, there are many proposals of fractal structures. The most common one that is widely used in many multiband applications is the Sierpinski carpet antenna array [3]. Other structures include cantor [4], hexagonal, pentagonal [5], Piano-Gosper space-filling curve [6], Minkowski island, and Koch loop [7]. These conventional fractal arrays contain numerous inactive elements in their design, depending on the initial array structure known as a generator. Thus, they usually suffer from the highest sidelobes, lowest directive gain, and poorer taper efficiency [1]. These undesirable features are caused by the fact that amplitude distributions of the fractal array elements are only at ones and zeros. Ones mean that the array elements are in the active state (on), while zeros mean that the array elements are in the inactive state (off). To date, the usage of these types of the fractal arrays was limited solely to multiband applications in which high radiation characteristics are not of the main concern.

On the other hand, clustered antenna arrays are currently gaining a lot of interest due to their effectiveness in reducing complexity of the beamforming network of large antenna arrays, as well due to the fact that they are capable of maintaining good radiation characteristics [8]–[13]. In general, there is need to find, by means of an optimization algorithm, the optimal clustering/tiling configurations that guarantee complete coverage of the entire array apertures.

Currently, fractal shapes present in the designs are mostly built with individual array elements, and many of these elements are turned off at the final construction stage. Very few studies attempted to reduce the number of the off-state elements in the fractal array geometry by means of an optimization algorithm, in order to improve directivity and lower peak sidelobes [14]–[16].

In this paper, conventional fractal antenna arrays are redesigned with efficient clustered shapes used instead of the individual elements. To the best of the author's knowledge, fractal arrays are designed, for the very first time, jointly with clustered subarrays, thus creating a new array referred to as a clustered fractal array which may be characterized by highly simplified features. Such clustered shapes are chosen to make sure that the original fractal shapes and their multiband operation capabilities are maintained and remain unchanged. The proposed clustered fractal array not only reduces the complexity of the array feeding network, but also offers a significant improvement in radiation characteristics. A genetic optimization algorithm is used to find the optimal clustered fractal shapes and their associated amplitude distributions, such that an improvement in directivity, sidelobe pattern, and

taper efficiency may be ensured in comparison to the characteristics of the conventional, original fractal array without clustered elements.

2. Clustered Fractal Array

To generate a fractal array, an iterative procedure is proposed to replicate the initial structure (usually known as generator) several times over a variety of scales, with each stage of the design corresponding to a specific frequency band. Thus, the final solution is capable of operating in distinct multiband frequencies. In contrast, standard antenna arrays which are designed to match a given operation frequency can be tuned to a single band only.

To show the dependence of frequency on the array pattern, let us consider a two-dimensional rectangular array made up of a number of elements equal to $N \times M$ that are symmetrically distributed around the center of the array, along both x and y axes, with uniform inter-element spacing $d_x = d_y = \frac{\lambda_o}{2}$, where $\lambda_o = \frac{c}{f_o}$ and f_o is the design frequency. Clearly, this array is frequency dependent and its array factor changes with frequency as:

$$AF(u,v,f) = \sum_{n=1}^{N}\sum_{m=1}^{M} a_{nm} \mathrm{e}^{\mathrm{j}\rho_{nm}} \mathrm{e}^{\mathrm{j}[(m-1)\pi \frac{f}{f_o} u]} \mathrm{e}^{\mathrm{j}[(n-1)\pi \frac{f}{f_o} v]} \tag{1}$$

where:

a_{nm} and ρ_{nm} are the amplitudes and phases of the element distributions,

$u = \sin\theta\cos\phi$,

$v = \sin\theta\sin\phi$,

θ and ϕ are the elevation and azimuth planes respectively,

f is the frequency band other than the designed value,

$\frac{f}{f_o}$ ratio is the difference from the design frequency.

On the other hand, the general form of a two-dimensional fractal array factor at any construction stage, $p = 1, 2, \ldots, P$, may be written as:

$$AF_{fractal}(u,v,f) = \prod_{p=1}^{P} \left[\sum_{n=1}^{N}\sum_{m=1}^{M} a_{nm} \mathrm{e}^{\mathrm{j}\rho_{nm}} \times \mathrm{e}^{\mathrm{j}[4^{p-1}(m-1)\pi \frac{f}{f_o} u]} \mathrm{e}^{\mathrm{j}[4^{p-1}(n-1)\pi \frac{f}{f_o} v]} \right]. \tag{2}$$

For the amplitude-only control method, element phase distributions are set to $\rho_{nm} = 0$ and the values of fractal amplitude distributions a_{nm} are at two levels only, namely one and zero, depending on the initial fractal generator used.

For example, let us assume that the initial linear array generator at the first stage is `0110`, where the number of active and inactive elements is 2. Then, for the next stages of the fractal construction process, each `1` is replaced by `0110` and each `0` by `0000` to form a new, larger amplitude distribution of `0000011001100000` at the second stage of the fractal construction, and so on. The number of active elements at the second stage becomes 4, while the number of inactive elements becomes 12. For the two-dimensional Sierpinski carpet array, the initial fractal subarray geometry at the first stage may be given by:

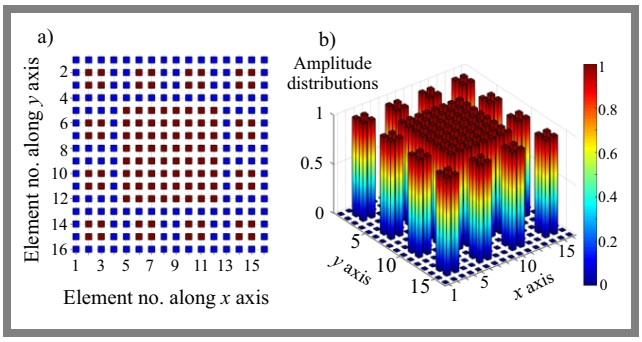

Fig. 1. Original Sierpinski carpet fractal array: a) layout and b) amplitude distribution.

$$a_{nm} = \begin{bmatrix} 0 & 0 & 0 & 0 \\ 0 & 1 & 1 & 0 \\ 0 & 1 & 1 & 0 \\ 0 & 0 & 0 & 0 \end{bmatrix}. \tag{3}$$

Note that the initial fractal array generator could be of any form that may be replicated over many design stages, until the final fractal geometry is obtained. Fractal amplitude distributions at the second stage of the construction process may be obtained by the following iterative steps:

1: $a_{nm} = 0$

2: $P = 2$

3: **For** $k = 1$ **to** P

4:

$$a_{nm} = \begin{bmatrix} a_{nm} & a_{nm} & a_{nm} & a_{nm} \\ a_{nm} & \mathrm{ones}\,4^{(k-1)} & \mathrm{ones}\,4^{(k-1)} & a_{nm} \\ a_{nm} & \mathrm{ones}\,4^{(k-1)} & \mathrm{ones}\,4^{(k-1)} & a_{nm} \\ a_{nm} & a_{nm} & a_{nm} & a_{nm} \end{bmatrix} \tag{4}$$

5: **End for**

By applying Eqs. (3) and (4), the amplitude distribution of the conventional, original Sierpinski carpet fractal array can be obtained as shown in Fig. 1 for $N \times M = 16 \times 16$ elements. Blue blocks represent active elements that are turned on and red blocks represent inactive elements that are turned off.

The multiband frequencies of fractal antenna arrays can be given by [2]:

$$f_p = \frac{f_o}{\delta^p}, \quad p = 0, 2, \ldots, P-1\,, \tag{5}$$

where δ is the number of elements in the initial linear fractal generator, here equaling 4. For the first stage of the design process, the tuned frequency is f_o. For other consecutive stages, the turning frequencies are f_o, $\frac{f_o}{4}$, $\frac{f_o}{16}$, $\frac{f_o}{256}$ and so on.

To join the fractal principles with the clustered subarrays mechanism, first we divide the inactive elements of the original fractal array into multiple square ring subarrays, starting with the elements on the array's perimeter, all the way to the

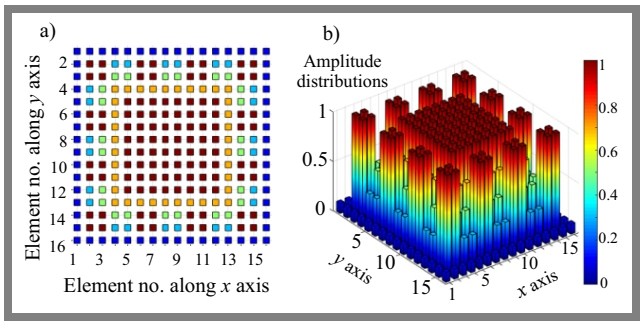

Fig. 2. Proposed clustered fractal array: a) square ring layout and b) amplitude distributions.

center of the array, as shown in Fig. 2, where each square-ring has been highlighted with different colors. The exact number of the elements in each square ring, K_r, can be determined by:

$$K_r = 2\big[2r(N-r)\big] - 2\big[2(r-1)(N-r+1)\big], \quad r = 1, 2, \ldots, R, \tag{6}$$

where R is the total number of square rings available in the considered array.

Then, a new common adjustable amplitude weight is attached to each clustered square-ring. Thus, amplitude distributions will be computed at the clustered level, rather than at the level of individual elements.

Next, the amplitude distribution of each clustered square ring is optimized, such that its corresponding array factor obeys a specific constraint mask with the desired sidelobe level and main beamwidth. To keep the original fractal geometry unchanged, amplitude distributions of the active elements (i.e. those elements whose magnitude equals one) of the original Sierpinski carpet array are left unchanged, i.e. remain at one (see Figs. 1–2). As none of the elements remain inactive after the process of optimizing the clustered fractal array, taper efficiency and directivity are expected to be improved when compared to those of the original Sierpinski carpet array. The genetic algorithm is used to optimize clustered amplitude distributions of the proposed fractal square ring elements, according to the following cost function:

$$cost = \sum_{s=1}^{S} \left| AF_{fractal}(u_s) - constraint\_mask(u_s) \right|^2, \tag{7}$$

where the constraint mask is given by:

$$constraint\_mask(u) = \begin{cases} SLL, & -1 \leqslant u \leqslant -\frac{BW}{2} \\ & \frac{BW}{2} \leqslant u \leqslant 1 \\ 0, & -\frac{BW}{2} \leqslant u \leqslant BW \end{cases}, \tag{8}$$

where BW and SLL represent the desired beamwidth and the sidelobe level.

3. Simulation Results

In this section, several simulation results are presented and discussed to assess the validity, efficiency, and reliability of

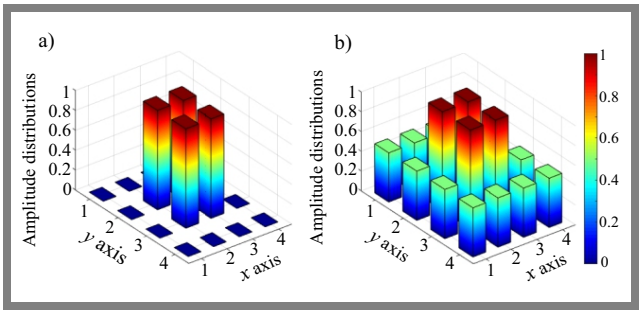

Fig. 3. Amplitude distributions: a) original Sierpinski carpet fractal array and b) optimized clustered fractal array.

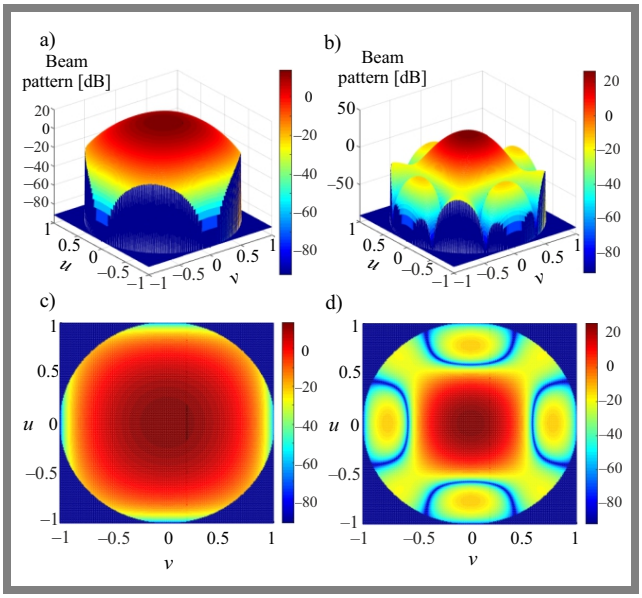

Fig. 4. Three-dimensional radiation patterns of the original Sierpinski carpet fractal array a), c) and optimized clustered fractal array b), d).

the proposed clustered fractal array. In all the representative examples, the following specifications of the genetic algorithm were used:

- initial population size of 50,
- number of iterations set to 1000,
- selection is roulette,
- number of crossovers is 2,
- mutation probability is 0.04,
- mating pool is chosen to be 4.

In the first example, the performance of the proposed array with $N \times N = 4 \times 4$ elements at the first stage of the fractal design is presented. The amplitude distribution of the original Sierpinski carpet array was given in Eq. (3). To find the optimized value of the clustered amplitude distribution of each subarrayed square ring A_r its minimum and maximum values are bound according to the following limits:

$$0 \leqslant A_r \leqslant 1, \quad r = 1, 2, \ldots, R. \tag{9}$$

For an array with $N \times N = 4 \times 4$ elements, $R = 1$. To keep the original fractal geometry, the amplitude distribution of the central elements should remain, according to Eq. (3), at

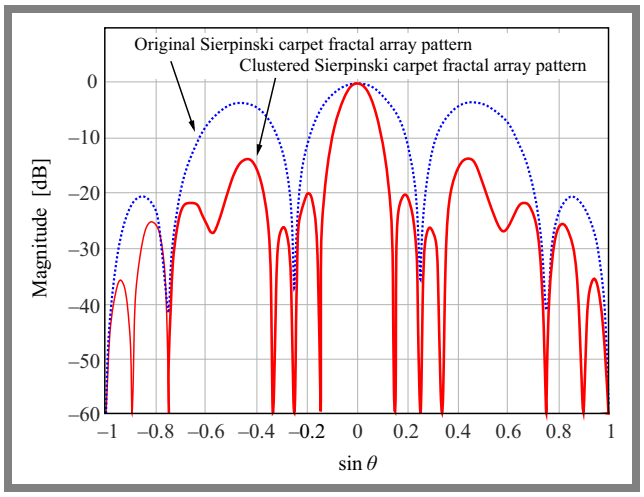

Fig. 5. Two-dimensional radiation patterns of the original and clustered Sierpinski carpet fractal array.

one, while optimizing the clustered amplitude distribution of the first square ring A_1 as:

$$a_{nm} = \begin{bmatrix} A_1 & A_1 & A_1 & A_1 \\ A_1 & 1 & 1 & A_1 \\ A_1 & 1 & 1 & A_1 \\ A_1 & A_1 & A_1 & A_1 \end{bmatrix}.$$

Note that the optimization process contains only one variable at the clustered level which can be easily optimized according to the required constraint mask given in Eq. (7). Figure 2 shows the amplitude distributions of the original and the optimized clustered Sierpinski carpet fractal arrays at the first stage of the construction process, while Figs. 4–5 show their corresponding three- and two-dimensional radiation patterns. From Fig. 3, the optimized value of the clustered amplitude distribution of the first square ring was $A_1 = 0.4981$. From Figs. 4–5, it can be seen that directivity and the sidelobe pattern of the proposed clustered array are much better than those of the original Sierpinski carpet fractal array, with directivity improvement exceeding 9.5 dB and sidelobe reduction being higher than –10 dB.

Other outcomes of the performance comparison process are shown in Tab. 1, while the frequency responses of the proposed clustered array and the original fractal array, both at stage $P = 1$, are shown in Fig. 6. Here, the designed frequency was 30 GHz and the tested range was from 1 GHz to 30 GHz. It can be seen that the proposed fractal array pattern performs very well within the majority of the frequency range.

In the second example, the plots of Figs. 7–8 show the results of the original and the optimized clustered Sierpinski carpet fractal arrays at the second stage of the fractal construction process. Here, 4 different clustered square rings are present. Their optimized values are $A_1 = 0.8505$, $A_2 = 0.7857$, $A_3 = 0.6451$, $A_4 = 0.6182$. It can be seen that, as the design stage progresses, performance of the proposed clustered fractal array becomes better due to the availability of more square rings around the array center, which directly contributes to an increase in the number of the clustered amplitude distributions or the number of degrees of freedom in the optimization algorithm.

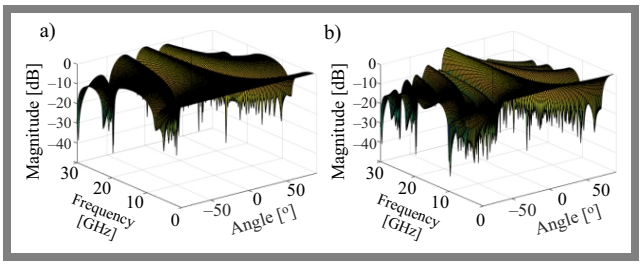

Fig. 6. Frequency responses: original Sierpinski carpet fractal array a) and optimized clustered fractal array b).

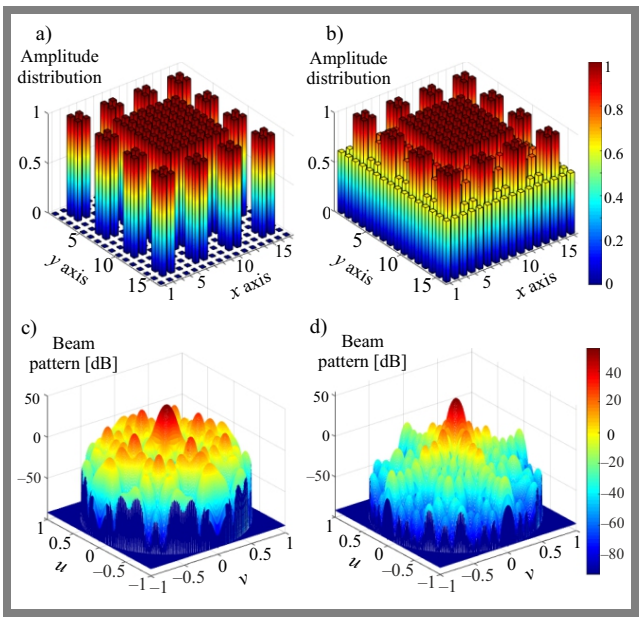

Fig. 7. Amplitude distributions and their corresponding radiation patterns for original Sierpinski carpet fractal array a), c) and optimized clustered fractal array b), d).

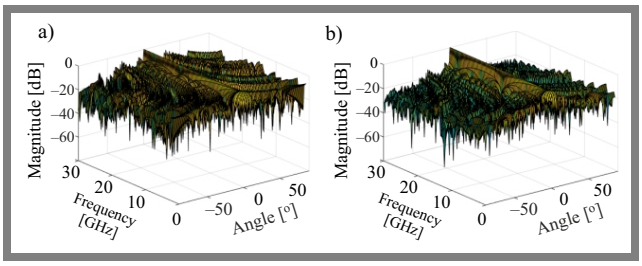

Fig. 8. Frequency responses: original Sierpinski carpet fractal array: a) and optimized clustered fractal array b).

In the next example, the capability of placing a wide sidelobe nulling capability at the elevation plane from the range of $u = \pm 0.3$ to ± 0.4 is investigated with the depth depressed to more than –60 dB. In this case, the amplitude distribution of each inactive element of the original Sierpinski carpet array is optimized individually. The optimized and the original radiation patterns of the Sierpinski carpet fractal arrays at second stage of construction are shown in Fig. 9. The corresponding optimized amplitude distribution is also shown in this figure.

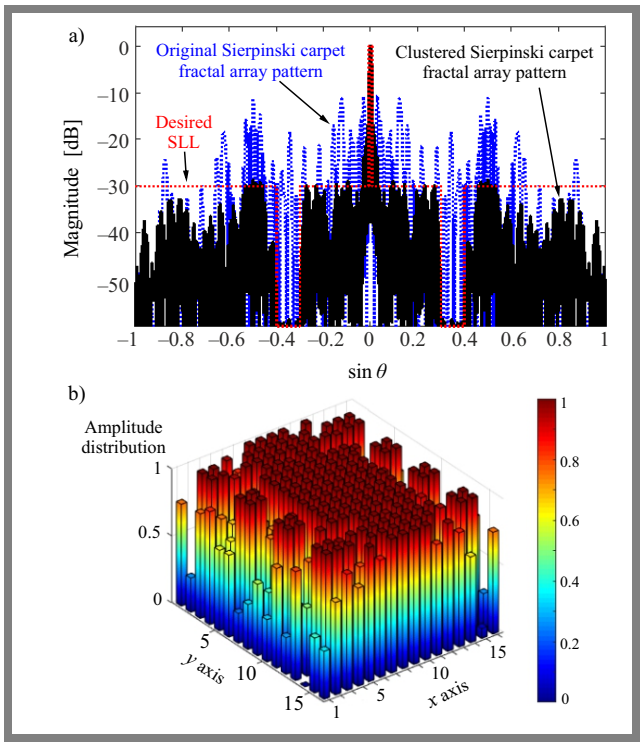

Fig. 9. Wide sidelobe nulling capability: a) radiation patterns and b) optimized amplitude distributions.

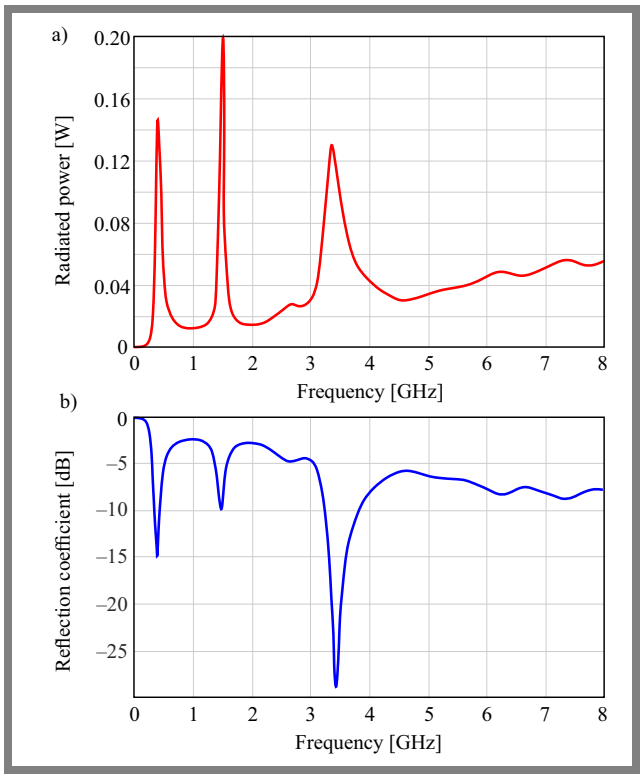

Fig. 10. Multiband operation capability: (a) radiated power (b) reflection coefficient.

Finally, a simple model of the proposed fractal array is designed with the operating frequency of 3.5 GHz and is examined for second-stage multiband operation capability at 3.5 GHz, 1.5 GHz, and 0.4 GHz frequencies, where the radiated power as well as the reflection coefficient are calculated within the frequency of 0.1 to 8 GHz, as shown in Fig. 10. One may notice that the designed fractal array has 3 resonance frequencies, where the radiated power is at its maximum and the reflection coefficient is at its minimum. The first resonance is at the designed frequency of 3.5 GHz. The second resonance is at 1.5 GHz, which corresponds to the first stage of the fractal design process, while the third resonance is at 0.4 GHz, which corresponds to the second stage of the fractal design process.

4. Conclusions

In this paper, a novel clustering configuration for rearranging the array elements of Sierpinski carpet fractal planar arrays is proposed. The method is based on the formation of clustered amplitude weights, rather than on dealing with the individual elements. Since the fractal geometry was retained after clustering, the multiband operation capability was maintained as well, and many other desired characteristics, such as directivity improvement, better sidelobe reduction, and efficient taper efficiency, could be achieved. To obtain such desired radiation patterns, the amplitude distributions of the fractal square-rings are elegantly clustered and optimized.

It has been shown that the proposed clustered fractal array with optimized square ring amplitude distributions achieves lower sidelobe levels, higher directivity and better taper efficiency compared with the parameters of conventional fractal arrays without clustered elements. Moreover, the proposed method can be applied to other fractal antenna arrays in order to simplify their construction process, while achieving good radiation characteristics.

References

[1] D.H. Werner, R.L. Haupt, and P.L. Werner, "Fractal Antenna Engineering: The Theory and Design of Antenna Arrays", *IEEE Antennas and Propagation Magazine*, vol. 41, no. 5, pp. 37–58, 1999 (https://doi.org/10.1109/74.801513).

[2] S.E. El-Khamy, H.F. EL-Sayed, and A.S. Eltrass, "A New Adaptive Beamforming of Multiband Fractal Antenna Array in Strong-Jamming Environment", *Wireless Personal Communications*, vol. 126, pp. 285–304, 2022 (https://doi.org/10.1007/s11277-022-09745-4).

[3] A. Karmakar, R. Ghatak, R.K. Mishra, and D.R. Poddar, "Sierpinski Carpet Fractal-based Planar Array Optimization Based on Differential Evolution Algorithm", *Journal of Electromagnetic Waves and Applications*, vol. 29, no. 2, pp. 247–260, 2015 (https://doi.org/10.1080/09205071.2014.997837).

[4] C. Puente-Baliarda and R. Pous, "Fractal Design of Multiband and Low Side-lobe Arrays", *IEEE Transactions on Antennas and Propagation*, vol. 44, no. 5, pp. 730–739, 1996 (https://doi.org/10.1109/8.496259).

[5] A. Karmakar, "Fractal Antennas and Arrays: A Review and Recent Developments", *International Journal of Microwave and Wireless Technologies*, vol. 13, no. 2, pp. 173–197, 2021 (https://doi.org/10.1017/S1759078720000963).

[6] D.H. Werner, W. Kuhirun, and P.L. Werner, "The Peano-Gosper Fractal Array", *IEEE Transactions on Antennas and Propagation*, vol. 51, no. 8, pp. 2063–2072, 2003 (https://doi.org/10.1109/TAP.2003.815411).

[7] C.A. Balanis, *Antenna Theory, Analysis, and Design*, 4th ed., Hoboken: Wiley, 1096 p., 2016 (ISBN: 9781118642061).

Tab. 1. Performance measures and comparison for the tested arrays under various conditions.

Methods	Stage	BFN*	Directivity [dB]	Taper efficiency	Peak SLL [dB]	Average SLL [dB]
Ordinary uniform amplitude distribution array	—	0	20.389	1	–13.2	–12.0766
	—	0	44.256	1	–13.2	–21.0511
Original Sierpinski carpet fractal array [1]	$P = 1$	0	10.098	0.25	–4	–10.0683
	$P = 2$	0	38.159	0.437	–10	–14.2962
Fully optimized Sierpinski carpet fractal array elements [13]	$P = 1$	12	18.054	0.7766	–20	–15.5655
	$P = 2$	114	43.658	0.9136	–30	–19.0267
Clustered Sierpinski carpet fractal array	$P = 1$	1	19.557	0.8916	–12	–11.6464
	$P = 2$	4	43.975	0.9633	–23	–20.3217
*Beamforming network (BFN) represents the needed number of the variable RF attenuators that attached to each active array elements.						

[8] P. Rocca, G. Oliveri, R.J. Mailloux, and A. Massa, "Unconventional Phased Array Architectures and Design Methodologies – A Review", *Proceedings of the IEEE*, vol. 104, no. 3, pp. 544–560, 2016 (https://doi.org/10.1109/JPROC.2015.2512389).

[9] J.R. Mohammed, "Minimizing Grating Lobes in Large Arrays Using Clustered Amplitude Tapers", *Progress in Electromagnetics Research C*, vol. 120, pp. 93–103, 2022 (https://doi.org/10.2528/PIERC22031706).

[10] H. Jiang, Y. Gong, J. Zhang, and S. Dun, "Irregular Modular Subarrayed Phased Array Tiling by Algorithm X and Differential Evolution Algorithm", *IEEE Antennas and Wireless Propagation Letters*, vol. 22, no. 7, pp. 1532–1536, 2023 (https://doi.org/10.1109/LAWP.2023.3250260).

[11] J.R. Mohammed, A.J. Abdulkadeer, and R. Hamdan, "Antenna Pattern Optimization via Clustered Arrays", *Progress in Electromagnetics Research M*, vol. 95, pp. 177–187, 2020 (https://doi.org/10.2528/PIERM20042307).

[12] R.J. Mailloux, S.G. Santarelli, T.M. Roberts, and D. Luu, "Irregular Polyomino-shaped Subarrays for Space-based Active Arrays", *International Journal of Antennas and Propagation*, vol. 2009, art. no. 956524, 2009 (https://doi.org/10.1155/2009/956524).

[13] J.R. Mohammed and K.H. Sayidmarie, "Sensitivity of the Adaptive Nulling to Random Errors in Amplitude and Phase Excitations in Array Elements", *Journal of Telecommunication, Electronic and Computer Engineering*, vol. 10, no. 1, pp. 51–56, 2018 (https://jtec.utem.edu.my/jtec/article/view/2023).

[14] V.A.S. Ponnapallia and P.V.Y. Jayasreeb, "Thinning of Sierpinski Fractal Array Antennas Using Bounded Binary Fractal-tapering Techniques for Space and Advanced Wireless Applications", *ICT Express*, vol. 5, no. 1, pp. 8–11, 2019 (https://doi.org/10.1016/j.icte.2017.12.006).

[15] K. Siakavara, "Novel Fractal Antenna Arrays for Satellite Networks: Circular Ring Sierpinski Carpet Arrays Optimized by Genetic Algorithms", *Progress in Electromagnetics Research*, vol. 103, pp. 115–138, 2010 (https://doi.org/10.2528/PIER10020110).

[16] J.R. Mohammed, "A Method for Thinning Useless Elements in the Planar Antenna Arrays", *Progress in Electromagnetics Research Letters*, vol. 97, pp. 105–113, 2021 (https://doi.org/10.2528/PIERL210221040).

Jafar Ramadhan Mohammed, Ph.D., Professor
College of Electronics Engineering
https://orcid.org/0000-0002-8278-6013
E-mail: jafar.mohammed@uoninevah.edu.iq
Ninevah University, Mosul, Iraq
https://uoninevah.edu.iq

Dalia Ahmad Al-Khafaf, B.Sc.
College of Electronics Engineering
daliaahmadalkhafaff@gmail.com
E-mail: dalia.khafaf@uoninevah.edu.iq
Ninevah University, Mosul, Iraq
https://uoninevah.edu.iq